Inorganic Chemistry

Article

pubs.acs.org/IC

Synthesis and Characterization of the Crystal and Magnetic Structures and Properties of the Hydroxyfluorides Fe(OH)F and Co(OH)F

Hamdi Ben Yahia,*[,†] Masahiro Shikano,*[,†] Mitsuharu Tabuchi,[†] Hironori Kobayashi,[†] Maxim Avdeev,[‡] Thiam Teck Tan,[§] Samuel Liu,[⊥] and Chris D. Ling[⊥]

[†]Research Institute for Ubiquitous Energy Devices, National Institute of Advanced Industrial Science and Technology (AIST), 1-8-31 Midorigaoka, Ikeda, Osaka 563-8577, Japan

[‡]Bragg Institute, B87, Australian Nuclear Science and Technology Organisation, Locked Bag 2001, Kirrawee DC, New South Wales 2232, Australia

[§]School of Materials Science and Engineering, University of New South Wales, Sydney, New South Wales 2052, Australia

[⊥]School of Chemistry, The University of Sydney, Sydney, New South Wales 2006, Australia

Supporting Information

ABSTRACT: The title compounds were synthesized by a hydrothermal route from a 1:1 molar ratio of lithium fluoride and transition-metal acetate in an excess of water. The crystal structures were determined using a combination of powder and/or single-crystal X-ray and neutron powder diffraction (NPD) measurements. The magnetic structure and properties of Co(OH)F were characterized by magnetic susceptibility and low-temperature NPD measurements. M(OH)F (M = Fe and Co) crystallizes with structures related to diaspore-type α-AlOOH, with the *Pnma* space group, $Z = 4$, $a = 10.471(3)$ Å, $b = 3.2059(10)$ Å, and $c = 4.6977(14)$ Å and $a = 10.2753(3)$ Å, $b = 3.11813(7)$ Å, and $c = 4.68437(14)$ Å for the iron and cobalt phases, respectively. The structures consist of double chains of edge-sharing $M(F,O)_6$ octahedra running along the *b* axis. These infinite chains share corners and give rise to channels. The protons are located in the channels and form O−H···F *bent* hydrogen bonds. The magnetic susceptibility indicates an antiferromagnetic ordering at ∼40 K, and the NPD measurements at 3 K show that the ferromagnetic rutile-type chains with spins parallel to the short *b* axis are antiferromagnetically coupled to each other, similarly to the magnetic structure of goethite α-FeOOH.

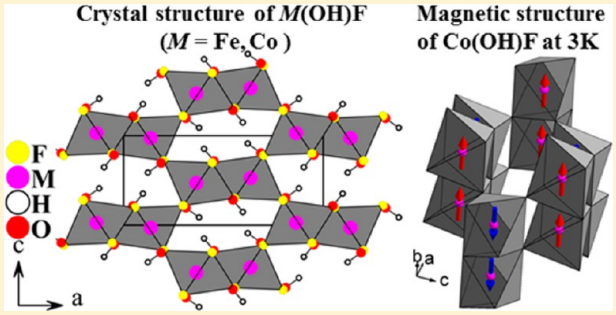

1. INTRODUCTION

The manganese dioxides MnO_2 are well-known to exhibit several structural forms. Among them, the mineralogical β-MnO_2 (pyrolusite, $P4_2/mnm$, $a = 4.388$ Å, $c = 2.865$ Å) and MnO_2 (ramsdellite, *Pnma*, $a = 9.2734$ Å, $b = 2.8638$ Å, $c = 4.5219$ Å) are the most stable.[1,2] These forms are isostructural to rutile TiO_2 and diaspore α-AlOOH structures, respectively.[3,4] At relatively low pressure (0.3 GPa), a second-order phase transition occurs from β-MnO_2 to $CaCl_2$-type MnO_2 form ($CaCl_2$ type, *Pnnm*, $a = 4.312$ Å, $b = 4.437$ Å, $c = 2.862$ Å), which crystallizes with a distorted rutile structure.[5] At 46 GPa, $CaCl_2$-type MnO_2 transforms to a cubic phase ($a = 4.484$ Å) similar to SiO_2 ($Pa\bar{3}$ or $Fm\bar{3}m$).[5] A few other MnO_2 synthetic forms have also been prepared, such as α-MnO_2 (hollandite, $I4/m$, $a = 9.7876$ Å, $c = 2.865$ Å) or λ-MnO_2 (spinel, $Fd\bar{3}m$, $a = 8.03$ Å), obtained by the precipitation method and electrochemical lithium deintercalation from the spinel $LiMn_2O_4$ phase (spinel, $Fd\bar{3}m$, $a = 8.24$ Å), respectively.[6,7]

In pyrolusite, $CaCl_2$-type, and ramsdellite, hexagonal-close-packed arrays of oxygen atoms are observed, whereas the spinel has cubic-close-packed oxygen arrays. In all of these compounds, the manganese atoms are octahedrally coordinated. However, because the connectivity between these polyhedra is different, one- to three-dimensional empty channels have been observed (Figure 1). This structural feature has attracted considerable attention from electrochemists.[8−10] Indeed, because there is a need for high-performance electrode materials for high-power lithium-ion batteries (LIBs), several researchers have attempted to replace the graphite anode employed in practical electrodes (theoretical specific capacity of 372 mAh g^{-1}) by manganese dioxides (theoretical capacity of 1232 mAh g^{-1}). Furthermore, MnO_2 is intensively used in primary alkaline cells. The key reaction of MnO_2 in these cells is $MnO_2 + e^- + H^+ \rightarrow MnOOH$.[11] These manganese

Received: September 10, 2013
Published: December 16, 2013

   dx.doi.org/10.1021/ic402294g | *Inorg. Chem.* 2014, 53, 365−374

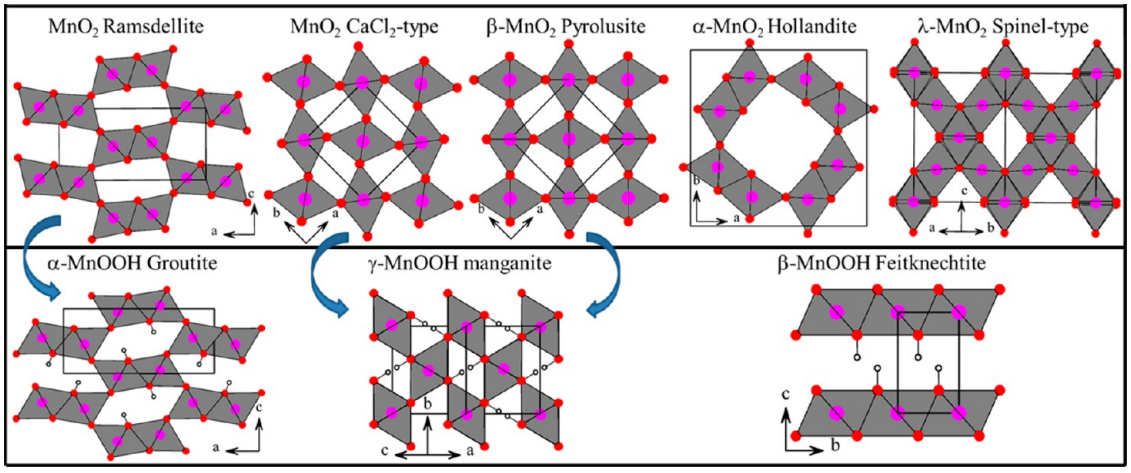

Figure 1. Structural relationship between the MnO_2 and MnOOH polymorphs.

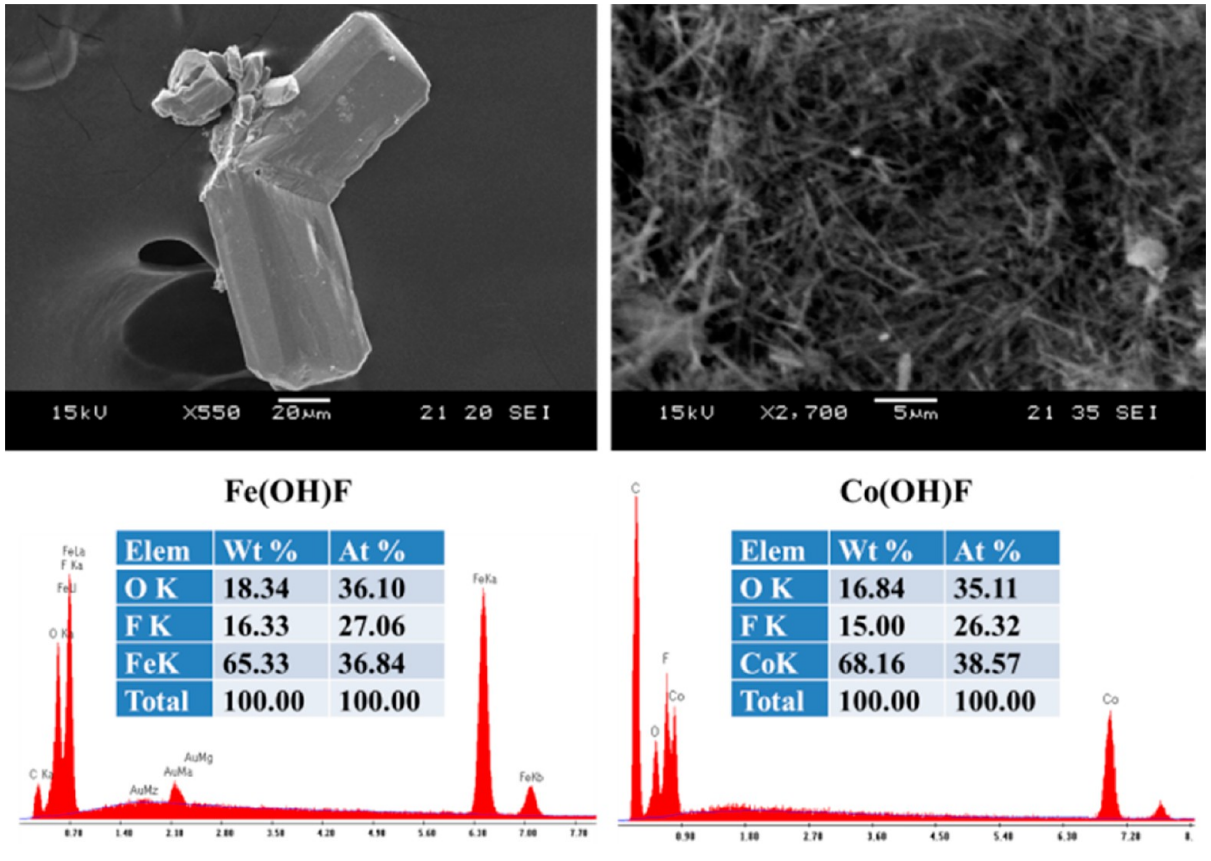

Figure 2. SEM images of Fe(OH)F twinned single crystals and Co(OH)F nanofibers.

oxyhydroxides MnOOH also exist in several modifications: the minerals α-MnOOH (groutite, *Pnma*, a = 10.667 Å, b = 2.871 Å, c = 4.554 Å) with the diaspore α-AlOOH structure; β-MnOOH (feitknechtite, $P\bar{3}m$, a = 3.32 Å, c = 4.71 Å) isotypic with pyrochroite $Mn(OH)_2$; γ-MnOOH (manganite, $P2_1/c$, a = 5.304 Å, b = 5.277 Å, c = 5.304 Å, β = 114.38°) with a modified rutile-type structure (Figure 1).[12−14] Synthetic MnOOH is the simplest and most practical precursors for the preparation of manganese oxides, intercalation compounds, and lithium manganese oxides for LIBs. When the trivalent manganese ion is replaced by a divalent transition-metal or alkali-earth-metal ion and one oxide ion is replaced by a fluoride ion, a homologous family of compounds is formed. The M(OH)F (M = Mg, Co, Ni, Cu, Zn, Cd, and Hg) compounds do indeed exist, and their crystal structures are strongly related to the α-, β-, and γ-MnOOH polymorphs.[15−23] Recently, during our attempts to synthesize the LiMOF (M = Mn, Fe, and Co) compositions, we obtained new M(OH)F compounds. The Fe(OH)F and Co(OH)F structures are related to the diaspore α-AlOOH structure, whereas Mn(OH)F crystallizes with a distorted rutile structure related to the $CaCl_2$ type.

In the present work, we report that we have synthesized the new compounds M(OH)F (M = Fe and Co) and solved their crystal structures using a combination of powder and/or single-crystal X-ray (XRD) and neutron powder diffraction (NPD) measurements. We have also characterized the Co(OH)F

dx.doi.org/10.1021/ic402294g | *Inorg. Chem.* 2014, 53, 365−374

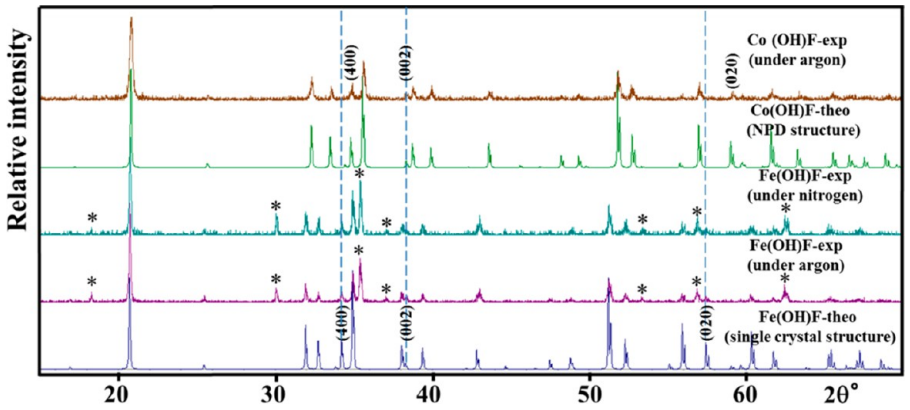

Figure 3. Powder XRD patterns of Fe(OH)F and Co(OH)F, obtained from hydrothermal syntheses. The asterisks correspond to Fe_3O_4 ($Fd\bar{3}m$, a = 8.408 Å).[25]

magnetic structure and properties by NPD and magnetic susceptibility measurements.

2. EXPERIMENTAL SECTION

2.1. Synthesis. Fe(OH)F and Co(OH)F were obtained by hydrothermal synthesis from a 1:1 molar ratio of lithium fluoride and transition-metal acetates. Each starting material was separately dissolved in 30 mL of distilled water, preheated at 50 °C. The two solutions were then mixed and left to stir for 1 h. The solutions were finally poured into 100 mL autoclaves, which were sealed in a glovebox under an argon or nitrogen atmosphere and heated at 200 °C for 48 h. By filtering the solutions, dark-green and pink powders were obtained for the iron and cobalt phases, respectively. An attempt to prepare Ni(OH)F under the same conditions led to $Ni(OH)_2$. It is worth pointing out that the amount of Co(OH)F powder obtained was much larger than that of Fe(OH)F, although the same preparation process was used.

The Fe(OH)F single crystals used for data collection were obtained from a 3:1 mixture of iron oxalate and lithium fluoride, which was fired at 200 °C for 60 h and then cooled slowly to room temperature at a rate of 15 °C h^{-1}. For Co(OH)F, no single crystals could be obtained even after a long treatment (2 weeks at 200 °C). Most of the Fe(OH)F single crystals were relatively large twinned needles, while the Co(OH)F powder consisted mostly of nanofibers (Figure 2).

2.2. Electron Microprobe Analysis. Semiquantitative energy-dispersive X-ray (EDX) analyses of the M(OH)F powders and single crystals, including the ones investigated on the diffractometer, were carried out with an EDAX Genesis analyzer installed on a JSM-5500LV (JEOL) scanning electron microscope. The experimentally observed compositions were close to the ideal M(OH)F (Figures 2 and S1 in the Supporting Information, SI). The Fe(OH)F powder contained a large amount of Fe_3O_4.

2.3. XRD. To ensure the purity of M(OH)F powders, routine powder XRD measurements were performed. Data were collected at room temperature over the range $5 \le 2\theta \le 80°$ with a step size of 0.01° on a RINT-TTR diffractometer (Rigaku) with monochromated Cu Kα radiation. Full pattern-matching refinements were performed with the *JANA2006* program package.[24] The background was estimated by a Legendre function, and the peak shapes were described by a pseudo-Voigt function. This revealed the presence of a large amount of Fe_3O_4 (45 wt %) in the samples prepared under argon and nitrogen (Figure 3). High-resolution powder XRD data using synchrotron radiation (λ = 0.5001 Å) were also collected on BL19B2 at SPring-8 [with the approval of the Japan Synchrotron Radiation Research Institute (Proposal No. 2012B1598)] for Co(OH)F (Figure S2 in the SI). Evaluation of these data yielded the refined cell parameters a = 10.29935(14) Å, b = 3.12808(4) Å, c = 4.69171(8) Å, and V = 151.154(5) $Å^3$.

Single crystals of Fe(OH)F suitable for XRD were selected on the basis of the size and sharpness of the diffraction spots. Data collection was carried out on a SMART APEX diffractometer using Mo Kα radiation. Data processing and all refinements were performed with the *JANA2006* program.[24] A Gaussian-type absorption correction was applied, and the shape was determined with a video microscope. For data collection details, see Table 1.

2.4. Magnetic Susceptibility Measurements. Magnetic susceptibility measurements of Co(OH)F were carried out using a Quantum

Table 1. Crystallographic Data and Structure Refinement Details for Fe(OH)F

formula	Fe(OH)F
cryst color	green-yellow
cryst size	0.120 × 0.055 × 0.028
M, g mol^{-1}	91.85
cryst syst	orthorhombic
space group	*Pnma*
a, Å	10.471(3)
b, Å	3.2059(10)
c, Å	4.6977(14)
V, $Å^3$	157.70(8)
Z	4
density calcd, g cm^{-3}	3.87
temperature, K	293(1)
F(000), e	176
diffractometer	SMART APEX
monochromator	graphite
radiation	Mo Kα, λ = 0.71069 Å
scan mode	multiscan
hkl range	$-9 < h < +13$
	$-4 < k < +3$
	$-6 < l < +5$
θ_{min}, θ_{max}, deg	3.89, 27.75
linear absorption coeff, mm^{-1}	9.067
abs corrn	Gaussian
T_{min}/T_{max}	0.647
no. of reflns	801
no. of indep reflns	212
reflns used	202
R_{int}	0.023
refinement	F^2
no. of refined param	20
R factors $R(F)/R_w(F^2)$	0.0211/0.0519
GOF	1.14
weighting scheme	$w = 1/[\sigma^2(I) + 0.0009I^2]$
diff Fourier residues max/min, e $Å^{-3}$	−0.27/+0.24

dx.doi.org/10.1021/ic402294g | *Inorg. Chem.* 2014, 53, 365−374

Table 2. Atom Positions, Equivalent Isotropic and Anisotropic ADPs for Fe(OH)F[a]

atom	Wyckoff	occupancy	x	y	z	U_{eq} (Å^2)
Fe1	4c	1	0.36438(4)	$^1/_4$	0.47205(11)	0.0141(2)
F1	4c	0.5	0.5567(10)	$^1/_4$	0.302(2)	0.0156(7)[b]
O1	4c	0.5	0.5478(13)	$^1/_4$	0.284(3)	0.0156(7)[b]
H1	4c	0.5	0.59718	$^1/_4$	0.14741	0.0156(7)[b]
F2	4c	0.5	0.2988(7)	$^3/_4$	0.2200(17)	0.0149(7)[b]
O2	4c	0.5	0.3119(9)	$^3/_4$	0.194(2)	0.0149(7)[b]
H2	4c	0.5	0.622(7)	$^1/_4$	0.912(18)	0.0149(7)[b]
atom	U_{11}	U_{22}	U_{33}	U_{12}	U_{13}	U_{23}
Fe1	0.0124(4)	0.0121(4)	0.0176(4)	0.00000	−0.00034(16)	0.00000

[a]The anisotropic ADP factor exponent takes the form $-2\pi^2[(ha^*)^2U_{11} + ... + 2hka\times b \times U_{12}]$. [b]$U_{iso}$.

Design Physical Properties Measurement System with a vibrating sample magnetometer probe. The susceptibility was recorded in the zero-field-cooled (ZFC) and 5 kOe field-cooled (FC) modes over the temperature range 2−300 K. Magnetization data as a function of the field were collected up to ±50 kOe at 5 K after the sample was cooled under a field of 50 kOe.

2.5. NPD. NPD data were collected on the high-resolution diffractometer Echidna at the OPAL facility (Lucas Height, Australia) using neutrons of wavelength 1.6215 Å. For the measurements, the sample in the form of ∼1 g of powder was loaded into a 6-mm-diameter cylindrical vanadium can and data were collected at 75 and 3 K, i.e., above and below the magnetic transition, using a closed-cycle refrigerator. Rietveld analysis of the data was performed using the *Fullprof* suite of programs with default neutron scattering lengths and a Co^{2+} magnetic form factor.[26]

3. RESULTS AND DISCUSSION

3.1. Structure Refinement. *3.1.1. Fe(OH)F Structure Refinement from Single-Crystal Data.* The extinction conditions observed for Fe(OH)F were compatible with the space groups *Pnma* (centrosymmetric) and $Pna2_1$ (non-centrosymmetric). The structure was solved in the space group *Pnma*. The three atomic positions forming the octahedral units were located using the superflip program implemented in *JANA2006*. At this stage, the chemical formula FeO_2 was in contradiction with EDX analysis, which shows the presence of a Fe/F/O mixture. Therefore, a F/O statistical disorder was introduced, and constraints on the anisotropic atomic displacement parameters (ADPs) and occupancies have been set [Occ(O) = 1 − Occ(F) and ADP(O) = ADP(F)]. The refinement then yields the chemical formula $FeF_{2-x}O_x$, and the structure is isotopic to the ramsdellite MnO_2 structure.[2] Because the iron ions are expected to be divalent, we suspected the presence of either xLi or xH in order to compensate for the excess of negative charges. The use of difference Fourier syntheses allowed us to localize the remaining proton positions on 4c sites with distances of around ∼0.85 Å from the O sites. When these positions were introduced and new constraints were set [Occ(H) = Occ(O) = 1 − Occ(F) and ADP(H) = ADP(O) = ADP(F)], the occupancies converged to values close to 0.5, but a large fluctuation of H1 was observed. Therefore, in the final refinement, the H1 position and the occupancies (0.5 for all atoms) were fixed. This led to the residual factors listed in Table 1. The refined atomic positions and ADPs are given in Table 2. Further details on the structure refinement may be obtained from Fachinformationszentrum Karlsruhe (Eggenstein-Leopoldshafen, Germany) by quoting the registry no. CSD-425870.

3.1.2. Co(OH)F Structure Refinement from NPD Data. The average Mg(OH)F crystal structure was used as a starting model for Rietveld refinement against Co(OH)F NPD data.[15] Initially, the protons were introduced in the structure as hydroxyl groups fully ordered with fluorine; however, difference Fourier maps clearly showed extra nuclear density located at ∼1 Å from the nominal fluorine position that strongly suggested partial (O,F) disorder. This was further supported by an improved agreement between the calculated and observed diffraction patterns after allowing partial F/OH disorder: R_p, R_{wp}, R_{Bragg}, and χ^2 were reduced from 1.77%, 2.42%, 12.0%, and 3.69 to 1.20%, 1.49%, 6.81%, and 1.41, respectively. Therefore, the model with partial F/OH disorder similar to that previously reported for ZnOHF[19] was used for further analysis of the NPD data. Because oxygen and fluorine atoms have very close neutron scattering lengths (b_c = 5.830 and 5.654 fm, respectively), the x value in $Co(OH)_xF_{2-x}$ could not be determined from refinement of the atomic occupancies for the common (O,F) site. However, because hydrogen is a relatively strong neutron scatterer (b_c = −3.74 fm), the refinement using constraints occ(H) = occ(O) = 1 − occ(F) for two inequivalent sites could be used to determine x quite precisely, resulting in the composition $Co(OH)_{0.86(3)}F_{1.14(3)}$. The final Rietveld plot and crystallographic information for $Co(OH)_{0.86(3)}F_{1.14(3)}$ at 300 and 75 K, i.e., in the paramagnetic state, are presented in Figure 4 and Table 3.

3.2. Crystal Structure. A projection view of the structure of Fe(OH)F, a derivative of the α-AlOOH diaspore structure, is displayed in Figure 5a, with the oxygen polyhedra drawn around the transition metals. The Fe(OH)F structure consists of double chains of edge-sharing $Fe(F,O)_6$ octahedra running along the b axis (Figure 5b). These infinite chains share corners

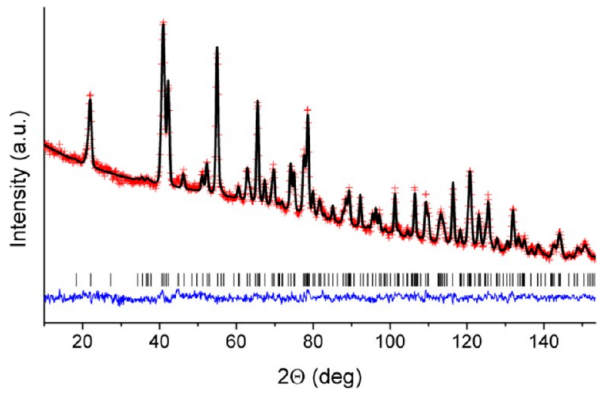

Figure 4. Rietveld plot for $Co(OH)_{0.86(3)}F_{1.14(3)}$ for the NPD data collected at 75 K, R_p = 1.20%, R_{wp} = 1.49%, R_{Bragg} = 6.81%, and χ^2 = 1.41.

dx.doi.org/10.1021/ic402294g | Inorg. Chem. 2014, 53, 365−374

Table 3. Crystal Structural Parameters for $Co(OH)_{0.86(3)}F_{1.14(3)}$ Based on the Rietveld Refinement against NPD Data Collected at 75 K [Space Group *Pnma* (No. 62), a = 10.2753(3) Å, b = 3.11813(7) Å, c = 4.68437(14) Å, V = 150.09(1) Å^3]

atom	Wyckoff	occupancy	x	y	z	B_{iso}, Å^2
Co	4c	1	0.3668(10)	$^1/_4$	0.4751(17)	0.94(10)
F1/O1	4c	0.658/0.342(10)	0.5521(4)	$^1/_4$	0.2938(9)	0.62(8)
H1	4c	occ(O1)	0.5723(14)	$^1/_4$	0.088(3)	B_{iso}(F1/O1)
F2/O2	4c	0.476/0.524(12)	0.3049(4)	$^3/_4$	0.2097(9)	0.72(7)
H2	4c	occ(O2)	0.6278(12)	$^1/_4$	0.9514(18)	B_{iso}(F2/O2)

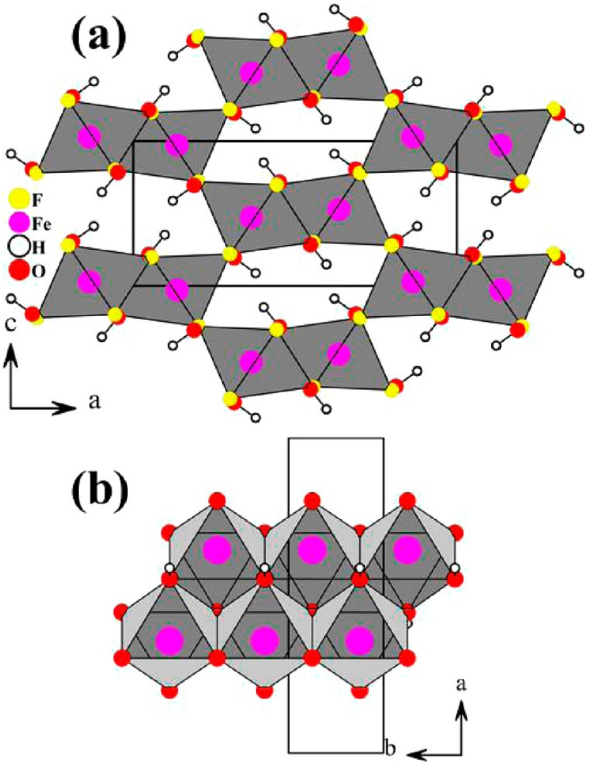

Figure 5. Projection views of the crystal structures of Fe(OH)F on the (010) plane and of the double chains of edge-sharing octahedra running along the b axis on the (001) plane. Thick solid blue lines emphasize the shape of the one-dimensional channels.

and give rise to tunnels in which the protons are located. Interatomic distances and bond valence sums (BVSs)[27,28] are listed in Table 4.

The $Fe(F,O)_6$ octahedra are distorted with F,O statistical disorder. The Fe−O distances range from 2.115 to 2.175 Å with an average value of 2.144 Å, whereas the Fe−F distances range from 2.068 to 2.167 Å with an average value of 2.106 Å. This leads to an average Fe−(O,F) distance of 2.125 Å. The BVS of 1.89 is in agreement with the expected value of 2 for Fe^{2+}.

The occurrence of short H1···H2, O1···H2, and O2···H1 distances of 1.13, 1.91, and 1.865 Å, respectively, may indicate serious structural problems (alert level A in Checkcif). However, these short distances can be well explained by the fluorine/oxygen statistical disorder. Simple distance considerations show that all of the (F/OH)···(HO/F) interactions are, in reality, OH···F hydrogen bonds, because, opposite to each hydroxyl group, there must be a fluorine atom. More details about the hydrogen-bonding geometries are depicted in Figure 6a−d.

Table 4. Interatomic Distances and BVSs for Fe(OH)F and $Co(OH)_{0.86(3)}F_{1.14(3)}$[a]

	Distance (Å)	BVS
Fe(OH)F-single crystal XRD at room temperature		
Fe1−O1	2.115(14)	0.357
Fe1−O2	2.120(10)	0.352
Fe1−O2 (× 2)	2.140(7)	0.334
Fe1−O1 (× 2)	2.175(9)	0.304
	<2.144>	1.985[b]
Fe1−F2	2.068(8)	0.331
Fe1−F1 (× 2)	2.094(7)	0.308
Fe1−F2 (× 2)	2.108(5)	0.297
Fe1−F1	2.167(11)	0.253
	<2.106>	1.794[b]
		<1.889>[b]
F1−O1	0.125(18)	
F2−O2	0.183(13)	
O1−H1	0.823(14)	
O2−H2	0.86(7)	
F2−H1	2.041(8)	
F1−H2	1.95(8)	
H1−H2	1.13(8)	
$CoF_{2-x}(OH)_x$ NPD at 75 K		
Co1−O1,F1 (× 2)	2.073(7)	0.357/0.318
Co1−O2,F2	2.079(11)	0.351/0.313
Co1−O1,F1	2.085(11)	0.346/0.308
Co1−O2,F2 (× 2)	2.093(6)	0.338/0.301
	<2.083>	<1.957>[b]
O1−H1	0.986(15)	
O2−H2	1.024(11)	
F1−H2	1.783(10)	
F2−H1	1.881(15)	
H1−H2	0.857(18)	

[a]Average distances are given in broken brackets. [b]BVS = $\exp[(r_0 - r)/b]$ with the following parameters: b = 0.37, $r_0(Fe^{II}-F)$ = 1.658, $r_0(Fe^{II}-O)$ = 1.734 Å, $r_0(Co^{II}-F)$ = 1.649, and $r_0(Co^{II}-O)$ = 1.692 Å.[27,28]

Starting from the disordered structure of Fe(OH)F, one may build at least three different ordered models. Because there are only two positions for the fluorine atoms (F1 and F2), we considered in the ordered model 1 that F^- and OH^- occupy sites 1 and 2, respectively. This induces the formation of a *bent* hydrogen bond with a F1···H2−O2 angle of 146.2° (Figure 6b). Inspection of the databases surprisingly revealed that such a hydrogen bond does not occur in any of the ordered oxyhydroxide MOOH or hydroxyfluoride M(OH)F compounds; however, it does occur in $Sr(OH)_2$ (*Pnma*, a = 9.8890 Å, b = 3.9184 Å, c = 6.1202 Å, V = 237.15 Å^3, and O1···H2−O2 angle =146.79°; Figure 6c).[29] It is worth noting that, although $Sr(OH)_2$ has been intensively studied, because all of the investigators used a coordination number of 7 for Sr^{2+}, they

dx.doi.org/10.1021/ic402294g | *Inorg. Chem.* 2014, 53, 365−374

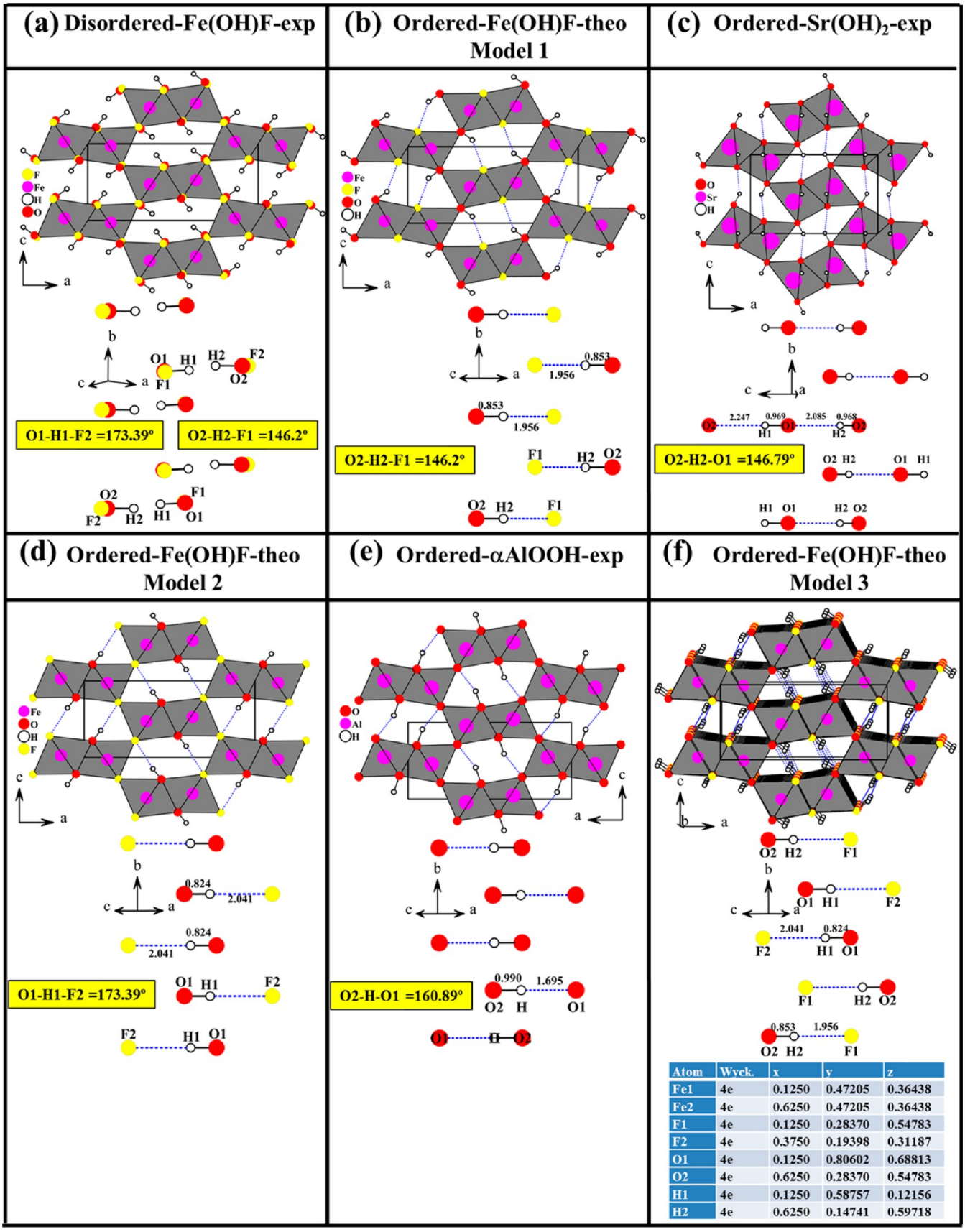

Atom	Wyck.	x	y	z
Fe1	4e	0.1250	0.47205	0.36438
Fe2	4e	0.6250	0.47205	0.36438
F1	4e	0.1250	0.28370	0.54783
F2	4e	0.3750	0.19398	0.31187
O1	4e	0.1250	0.80602	0.68813
O2	4e	0.6250	0.28370	0.54783
H1	4e	0.1250	0.58757	0.12156
H2	4e	0.6250	0.14741	0.59718

Figure 6. Views of the O,F disorder in the single-crystal structure (a) and theoretical O,F ordering in models 1 (b), 2 (c), and 3 (d).

could not see the strong structural relationship with the ramsdellite and diaspore structures. When we use a coordination number of 6 for Sr^{2+}, this relationship becomes obvious (Figure 6c,e).

dx.doi.org/10.1021/ic402294g | Inorg. Chem. 2014, 53, 365−374

In model 2, we considered that F^- and OH^- occupy sites 2 and 1, respectively. The resulting structure is isostructural to the diaspore-type structure (Figure 6d,e). Most of the oxyhydroxide compounds crystallize with this type of structure. However, there are large differences in the geometry of the *bent* hydrogen bond among these compounds. In Fe(OH)F, the F2···H1−O1 angle is 173.39°, while the O−H···H angles are 171.41, 160.89, and 152.36° in α-MnOOH, -αAlOOH, and α-GaOOH, respectively.[4,12,30]

In model 3, we attempted to alternate F^- and OH^- along the tunnels. Several steps were required to achieve this. The *Pnma* symmetry was first lowered to *P*1, and then the *b* cell parameter was doubled (a = 10.471 Å, b = 6.4118 Å, and c = 4.6977 Å), the OH^- and F^- anions were ordered one by one, and finally the 32 atomic positions were determined (Figure 6f). Finally, using the *PLATON* suite of crystallographic programs,[31] we determined that a higher-symmetry cell exists with the $P2_1/c$ space group, with parameters a = 6.4118 Å, b = 4.6977 Å, c = 10.471 Å, β = 90°, and Z = 8 and eight new atomic positions (Figure 6f).

The crystal structure of $Co(OH)_{0.86(3)}F_{1.14(3)}$ is very similar to that of Fe(OH)F. Interatomic distances and BVSs[27,28] are listed in Table 4. The $Co(O,F)_6$ octahedra are regular in shape. The Co−(O,F) distances range from 2.073 to 2.093 Å, with an average value of 2.083 Å slightly lower than the average value 2.1 Å estimated from the sum of the ionic radii of Co^{2+} (0.745 Å), F^- (1.31 Å), and O^{2-} (1.4 Å).[32] In $Co(OH)_{0.86(3)}F_{1.14(3)}$, *bent* hydrogen bonds occur with O2−H2···F1 and O1−H1···F2 angles of 163.37 and 150.01°, respectively.

Our three theoretical ordered models of Fe(OH)F may also be observed for the stoichiometric Co(OH)F compound. Among these three models, the probability of occurrence for model 3 appears to be much higher than that for models 1 or 2 because protons have been experimentally observed at distances from O1 and O2 between 0.85 and 1.00 Å. In models 1 and 2, the protons are attached only to O1 or O2.

Careful examination of different compounds with structures related to the ramsdellite-type structure (Table 5) revealed few differences. Indeed, the hexagonal-close-packed oxygen arrays are only slightly distorted in Fe(OH)F and Co(OH)F, whereas in the ramsdellite-type TiO_2 and especially in $Sr(OH)_2$, they are strongly distorted (Figure 7d−i). Such distortions induce the formation of tunnels with different shapes [i.e., parallelogram, rectangle, and elongated hexagon in Fe(OH)F, TiO_2, and $Sr(OH)_2$, respectively; Figure 7a−c].

3.3. Co(OH)F Magnetic Properties. The results of magnetic property measurements for Co(OH)F are presented in Figure 8. The molar magnetic susceptibility χ_m as a function of the temperature revealed a signature of a magnetic transition at $T \sim 40$ K. Above ~150 K, the corresponding $1/\chi_m$ curve follows the Curie−Weiss law. A linear fit in the range 200−300 K yielded $\Theta = -61.4$ K and an effective moment 5.39 μ_B, indicating predominantly antiferromagnetic (AFM) interactions in the system, with a substantial contribution from the unquenched orbital moment in addition to the spin-only value for d^7 Co^{2+}.

We attribute the observed ZFC/FC curve divergence at T_N and the weak ferromagnetic (FM) hysteresis at 2 K (Figure 8a) to the uncompensated moments from structural defects and on the particle surfaces (so-called superantiferromagnetism),[44] which can reasonably be expected for hydrothermally produced Co(OH)F. The phenomenon is well-known in AFM goethite FeOOH[45] and ferritin with AFM cores of $FeOOH{\cdot}xH_2O$.[46]

Table 5. Compounds with a Crystal Structure Related to the Diaspore- and Ramsdellite-Type Structures

compound	a (Å)	c (Å)	b (Å)	ref
diaspore α-AlO(OH)	9.4210	2.8450	4.4010	4
α-GaO(OH)	9.7907	2.9732	4.5171	30
groutite α-MnO(OH)	10.6670	2.8710	4.5540	12
groutellite $(MnO)_{1.5}(OH)_{0.5}$	9.5155	2.8644	4.706	2
α-ScO(OH)	10.3010	3.2090	4.7550	33
bracewellite CrO(OH)	9.860	2.974	4.492	34
montroseite VO(OH)	9.97	3.03	4.54	35
goethite α-FeO(OH)	9.956	3.0215	4.608	36
CoO(OH) HP	9.402	2.840	4.353	37
α-GaO(OD)	9.779	2.966	4.516	38
MgF(OH)	10.116	3.0794	4.6888	15
ZnF(OH)	10.228	3.1125	4.765	21
CoF(OH)	10.305	3.126	4.677	16
FeF(OH)	10.471	3.2059	4.6977	*a*
ramsdellite MnO_2	9.27	2.866	4.533	39
ramsdellite TiO_2	9.459	2.9585	4.9022	40
VO_2	9.39	2.93	4.89	41
CNb_2	10.76	3.135	4.966	42
$IrTe_2$	13.5116	4.0671	5.5275	43
$Sr(OH)_2$	9.8890	3.9184	6.1202	29

[a]From this work.

Magnetically, the bulk of such materials develop long-range order, while the surface demonstrates spin-glass behavior.[47] The latter results in a characteristic frequency dependence of the magnetic susceptibility, which was indeed confirmed in the present case by alternating-current (ac) susceptibility measurements (Figure S4 in the SI).

The shift of the hysteresis loop for the FC (5 T) sample (Figure 8b) also points to the presence of uncompensated spins on particle surfaces, resulting in an exchange-biased AFM/FM core−shell structure.[48] This has previously been observed in hydrothermally prepared goethite.[49] The similarity between the bulk magnetic structure of CoOHF and that of goethite FeOOH is discussed further below.

3.4. Co(OH)F Magnetic Structure from NPD Measurements. Examination of the NPD patterns collected at 3 and 75 K revealed additional diffraction peaks, presumably due to magnetic ordering. This is consistent with the magnetic susceptibility data, which suggested an AFM transition at ~40 K (Figure 8). All of the diffraction peaks of $Co(OH)_{0.86(3)}F_{1.14(3)}$ with magnetic contribution could be indexed by the crystallographic unit cell, i.e., with the propagation vector k = (0, 0, 0). For the 4c(x,0.25,z) Wyckoff site of the *Pnma* space group, the magnetic representation decomposes in terms of eight one-dimensional irreducible representations (IRs) as $\Gamma = \Gamma_1 + 2\Gamma_2 + 2\Gamma_3 + \Gamma_4 + \Gamma_5 + 2\Gamma_6 + 2\Gamma_7 + \Gamma_8$. The associated basis vectors are listed in Table S1 in the SI. The best agreement between the experimental and calculated powder diffraction patterns was obtained for the Γ_4 representation (equivalent to the *Pnma*′ Shubnikov group; Opechowski−Guccione number 62.5.506). The magnetic structure of $Co(OH)_{0.86(3)}F_{1.14(3)}$ can be described as AFM ordering of FM rutile-type chains of trans-edge-sharing octahedra with the moments parallel to the short *b* axis (Figure 9). It is qualitatively the same as that originally reported for goethite α-FeOOH,[50] which is not surprising because strong interchain superexchange dominates in the case of d^7 Co^{2+} in the same way that it does for the d^5 Fe^{3+} analogue, as expected

dx.doi.org/10.1021/ic402294g | Inorg. Chem. 2014, 53, 365−374

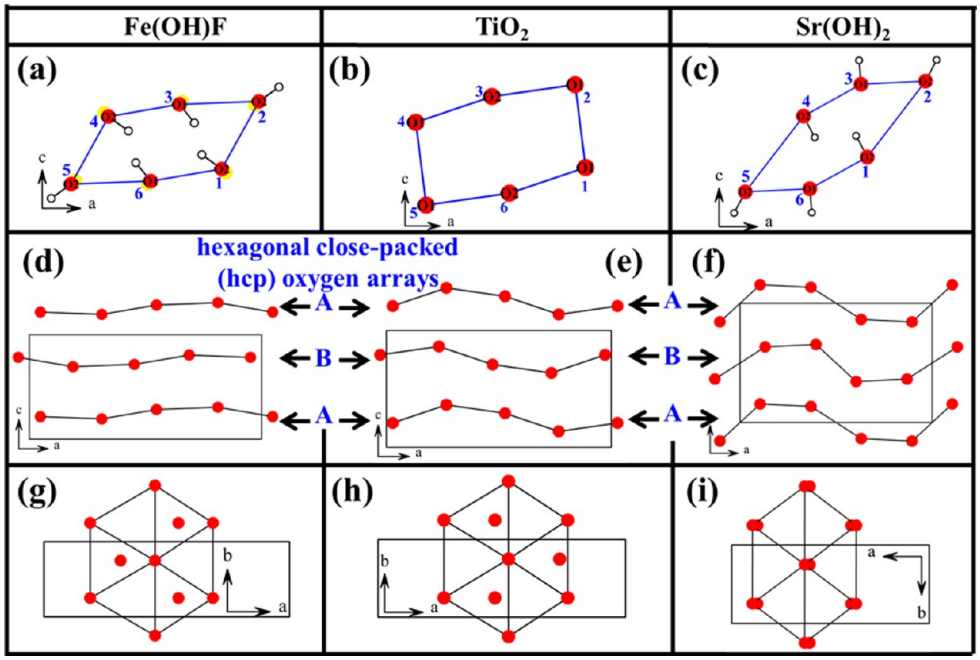

Figure 7. Distortion of the hexagonal-close-packed oxygen arrays in Fe(OH)F, ramsdellite-type-TiO_2, and $Sr(OH)_2$.

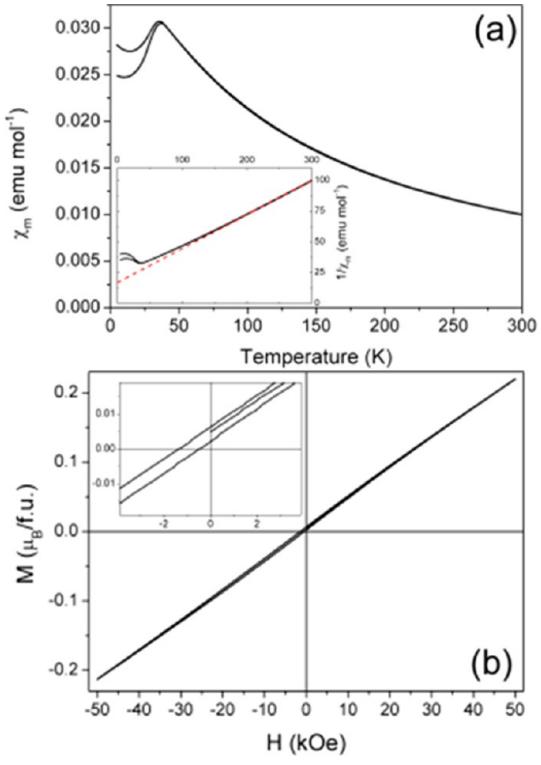

Figure 8. (a) Molar magnetic susceptibility χ_m of $Co(OH)_{0.86(3)}F_{1.14(3)}$ as a function of the temperature. The inset shows the corresponding $1/\chi_m$ and the linear fit with the Curie–Weiss function (red dashed line). (b) Magnetization M as a function of field H for a 50 kOe FC sample at 5 K.

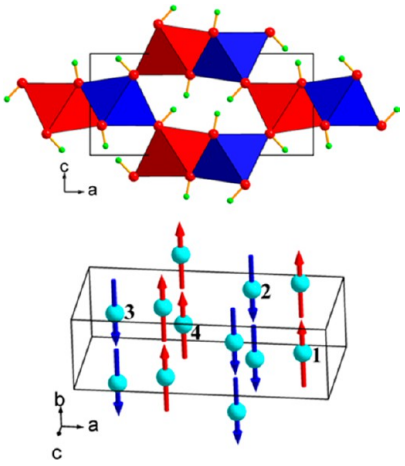

Figure 9. Magnetic structure of $Co(OH)_{0.86(3)}F_{1.14(3)}$ at 3 K. Top: red and blue octahedra showing cobalt sites with spins up and down, respectively. Bottom: same but with diamagnetic atoms omitted for clarity.

from the Goodenough–Kanamori rules.[51] Because one of the later studies of the magnetic structure of goethite suggested possible spin canting along the longest a axis,[52] we carefully tested the presence of such a magnetic mode but found no evidence of noncollinearity. We also note that an additional AFM mode allowing spin canting along the a axis would require mixing of basis vectors $\mathbf{A}_y$ and $\mathbf{G}_x$ of two IRs (Table S1 in the SI) and lowering of the magnetic symmetry to $P2_1'2_1'2_1$, which is unlikely given that there is no evidence that the magnetic transition in goethite is not second-order. Therefore, we concluded that our NPD data for $Co(OH)_{0.86(3)}F_{1.14(3)}$ supports the collinear model *Pnma*′. The final Rietveld plot and crystallographic information for the 3 K NPD data are presented in Figure S3 and Table S2 in the SI, respectively. The moment value determined for $Co(OH)_{0.86(3)}F_{1.14(3)}$ from the NPD data collected at 3 K, 2.41(3) μ_B, is significantly lower than the theoretical value for high-spin d^7 Co^{2+}, especially taking into account some contribution from an unquenched orbital moment, most likely due to chemical disorder of F and OH locally distorting Co–X–Co magnetic exchange paths (Table 4).

dx.doi.org/10.1021/ic402294g | *Inorg. Chem.* 2014, 53, 365–374

4. CONCLUSIONS

The new compounds Fe(OH)F and $Co(OH)_{0.86(3)}F_{1.14(3)}$ synthesized by a hydrothermal route were obtained serendipitously during preparation of the new phase LiMOF (M = Fe and Co). These compounds crystallize with distorted ramsdellite-type structures related to the well-known diaspore-type α-AlOOH. The structures consist of double chains of edge-sharing $M(F,O)_6$ octahedra running along the *b* axis. These infinite chains share corners, giving rise to infinite channels. Protons are located in the channels and form O−H···F *bent* hydrogen bonds. Magnetic susceptibility data for $Co(OH)_{0.86(3)}F_{1.14(3)}$ indicate AFM ordering below ∼40 K, and NPD measurements at 3 K show that FM rutile-type chains with spins parallel to the *b* axis are antiferromagnetically coupled to each other, similarly to the magnetic structure of goethite α-FeOOH.

■ ASSOCIATED CONTENT

Supporting Information

X-ray crystallographic data in CIF format, SEM images, plots for synchrotron powder XRD refinement, Rietveld plot, ac magnetic susceptibility, basis vectors for the 4c(0,0,0) site, and crystal structural parameters. This material is available free of charge via the Internet at http://pubs.acs.org.

■ AUTHOR INFORMATION

Corresponding Authors

*Tel: +81-72-751-7932. Fax: +81-72-751-9609. E-mail: benyahia.hamdi@voila.fr.

*Tel: +81-72-751-7932. Fax: +81-72-751-9609. E-mail: shikano.masahiro@aist.go.jp.

Notes

The authors declare no competing financial interest.

■ ACKNOWLEDGMENTS

This work was financially supported by a Grant-in-Aid for Japan Society for the Promotion of Science Fellows (Grant P 12506) and the Australian Research Council (Grant DP110102662).

■ REFERENCES

(1) Kondrashev, Y. D.; Zaslavskii, A. I. *Izv. Akad. Nauk SSSR (Ser. Fiz.)* **1951**, *15*, 179.
(2) Post, J. E.; Heaney, P. J. *Am. Mineral.* **2004**, *89*, 969.
(3) Legrand, C.; Delville, J. *C. R. Hebd. Seances Acad. Sci.* **1953**, *236*, 944.
(4) Busing, W. R.; Levy, H. A. *Acta Crystallogr.* **1958**, *11*, 798.
(5) Haines, J.; Léger, J. M.; Hoyau, S. *J. Phys. Chem. Solids* **1995**, *56*, 965.
(6) Rossouw, M. H.; Liles, D. C.; Thackeray, M. M.; David, W. I. F.; Hull, S. *Mater. Res. Bull.* **1992**, *27*, 221.
(7) Hunter, J. C. *J. Solid State Chem.* **1981**, *39*, 142.
(8) Kijima, N.; Takahashi, Y.; Akimoto, J.; Awaka, J. *J. Solid State Chem.* **2005**, *178*, 2741.
(9) Ling, C.; Mizuno, F. *Chem. Mater.* **2012**, *24*, 3943.
(10) Du, G.; Wang, J.; Guo, Z.; Chen, Z.; Liu, H. *Mater. Lett.* **2011**, *65*, 1319.
(11) Rogulski, Z.; Chotkowski, M.; Czerwinski, A. *J. New Mater. Electrochem. Syst.* **2006**, *9*, 401.
(12) Kohler, T.; Armbruster, T.; Libowitzky, E. *J. Solid State Chem.* **1997**, *133*, 486.
(13) Christensen, A. N.; Ollivier, G. *Solid State Commun.* **1972**, *10*, 609.
(14) Feitknecht, V. M.; Brunner, P.; Oswald, H. R. *Z. Anorg. Allg. Chem.* **1962**, *316*, 154.
(15) Crichton, W. A.; Parise, J. B.; Müller, H.; Breger, J.; Marshall, W. G.; Welch, M. D. *Mineral. Mag.* **2012**, *76*, 25.
(16) Rodriguez, M. A.; Millan, P.; Rojas, R. M.; Garcia, O. *J. Therm. Anal.* **1995**, *44*, 395.
(17) Lange, B. A.; Haendler, H. M. *J. Inorg. Nucl. Chem.* **1973**, *35*, 3129.
(18) Scholz, G.; Stosiek, C.; Feist, M.; Kemnitz, E. *Eur. J. Inorg. Chem.* **2012**, *14*, 2337.
(19) Peter, S.; Weckler, B.; Roisnel, T.; Lutz, H. D. *Bull. Chem. Technol. Macedonia* **1997**, *16*, 21.
(20) Giester, G.; Libowitzky, E. *Z. Kristallogr.* **2003**, *218*, 351.
(21) Serier, H.; Gaudon, M.; Demourgues, A.; Tressaud, A. *J. Solid State Chem.* **2007**, *180*, 3485.
(22) Stalhandske, C. *Acta Crystallogr.* **1979**, *B35*, 2184.
(23) Ben Yahia, H.; Shikano, M.; Kobayashi, H.; Avdeev, M.; Liu, S.; Ling, C. D. *Phys. Chem. Chem. Phys.* **2013**, *15*, 13061.
(24) Petricek, V.; Dusek, M.; Palatinus, L. *JANA2006. The crystallographic computing system*; Institute of Physics: Praha, Czech Republic, 2006.
(25) Okudera, H.; Kihara, K.; Matsumoto, T. *Acta Crystallogr.* **1996**, *B52*, 450.
(26) Rodriguez-Carvajal, J. *Phys. B* **1993**, *192*, 55.
(27) Brown, I. D.; Altermatt, D. *Acta Crystallogr.* **1985**, *B41*, 244.
(28) Brese, N. E.; O'Keefe, M. *Acta Crystallogr.* **1991**, *B47*, 192.
(29) Giese, R. F., Jr. *Z. Kristallogr.* **1977**, *146*, 205.
(30) Li, S. J.; Zheng, C.; Lobring, K. C. *Z. Kristallogr.* **2003**, *218*, 11.
(31) Spek, A. L. *PLATON, A Multipurpose Crystallographic Tool*; Utrecht University: Utrecht, The Netherlands, 2008.
(32) Shannon, R. D. *Acta Crystallogr., Sect. A: Cryst. Phys., Diffr., Theor. Gen. Crystallogr.* **1976**, *A32*, 751.
(33) Christensen, A. N.; Jensen, S. J. *Acta Chem. Scand.* **1967**, *21*, 121.
(34) Fleischer, M.; Cabri, L. J.; Nickel, E. H.; Pabst, A. *Am. Mineral.* **1977**, *62*, 593400.
(35) Evans, H. T.; Mrose, M. E. U.S. Geological Survey, Washington, DC.
(36) Sampson, C. F. *Acta Crystallogr.* **1969**, *B25*, 1683.
(37) Chevanas, J.; Joubert, J. C.; Capponl, J. J. *J. Solid State Chem.* **1973**, *6*, 1.
(38) Pye, M. F.; Birtill, J. J.; Dickens, P. G. *Acta Crystallogr.* **1977**, *B33*, 3224.
(39) Byström, A. M. *Acta Chem. Scand.* **1949**, *3*, 163.
(40) Akimoto, J.; Gotoh, Y.; Oosawa, Y.; Nonose, N.; Kumagai, T.; Aoki, K.; Takei, H. *J. Solid State Chem.* **1994**, *113*, 27.
(41) Evans, H. T., Jr.; Mrose, M. E. *Am. Mineral.* **1955**, *40*, 861.
(42) Alyamovskii, S. I.; Shveikin, G. P.; Gei, P. V. *Russ. J. Inorg. Chem.* **1963**, *8*, 1042.
(43) Jobic, S.; Brec, R.; Pasturel, A.; Koo, H. J.; Whangbo, M. H. *J. Solid State Chem.* **2001**, *162*, 63.
(44) Néel, L. *C. R. Acad. Sci.* **1962**, *252*, 4075.
(45) Liu, Q.; Torrent, J.; Yu, Y.; Deng, C. *J. Geophys. Res.* **2004**, *109*, B12106.
(46) Gilles, C.; Bonville, P.; Rakoto, H.; Broto, J. M.; Wong, K. K. W.; Mann, S. *J. Magn. Magn. Mater.* **2002**, *241*, 430.
(47) Laguta, V. V.; Glinchuk, M. D.; Marysko, M.; Kuzian, R. O.; Prosandeev, S. A.; Raevskaya, S. I.; Smotrakov, V. G.; Eremkin, V. V.; Raevski, I. P. *Phys. Rev. B* **2013**, *87*, 064403.
(48) Nogués, J.; Sort, J.; Langlais, V.; Skumryev, V.; Surinach, S.; Munoz, J. S.; Baró, M. D. *Phys. Rep.* **2005**, *422* (No. 3), 65.
(49) Barrero, C. A.; Betancur, J. D.; Greneche, J. M.; Goya, G. F.; Berquó, T. S. *Geophys. J. Int.* **2006**, *164*, 331.
(50) Forsyth, J. B.; Hedley, I. G.; Johnson, C. E. *J. Phys. (Paris)* **1968**, *C1*, 179.
(51) Goodenough, J. B. *Phys. Rev.* **1955**, *100*, 564. Kanamori, J. *J. Phys. Chem. Solids* **1959**, *10*, 87.
(52) Coey, J. M. D.; Barry, A.; Brotto, J.; Rakoto, H.; Brennan, S.; Mussel, W. N.; Collomb, A.; Fruchart, D. *J. Phys.: Condens. Matter* **1995**, *7* (no. 4), 759.

(53) Krezhov, K.; Petrov, K.; Karamaneva, T. *J. Solid State Chem.* **1983**, *48*, 33.

dx.doi.org/10.1021/ic402294g | *Inorg. Chem.* 2014, 53, 365−374